International Journal of Polymer Analysis and Characterization

ISSN: (Print) (Online) Journal homepage: https://www.tandfonline.com/loi/gpac20

Development and characterization of a novel activated biochar-based polymer composite for biosensors

Abdus Sobhan, Kasiviswanathan Muthukumarappan, Lin Wei, Quinn Qiao, Md Tawabur Rahman & Nabin Ghimire

To cite this article: Abdus Sobhan, Kasiviswanathan Muthukumarappan, Lin Wei, Quinn Qiao, Md Tawabur Rahman & Nabin Ghimire (2021) Development and characterization of a novel activated biochar-based polymer composite for biosensors, International Journal of Polymer Analysis and Characterization, 26:6, 544-560, DOI: 10.1080/1023666X.2021.1921497

To link to this article: https://doi.org/10.1080/1023666X.2021.1921497

Published online: 11 May 2021.

INTERNATIONAL JOURNAL OF POLYMER ANALYSIS AND CHARACTERIZATION
2021, VOL. 26, NO. 6, 544–560
https://doi.org/10.1080/1023666X.2021.1921497

Taylor & Francis
Taylor & Francis Group

Development and characterization of a novel activated biochar-based polymer composite for biosensors

Abdus Sobhan[a], Kasiviswanathan Muthukumarappan[a], Lin Wei[a], Quinn Qiao[b], Md Tawabur Rahman[b], and Nabin Ghimire[b]

[a]Department of Agricultural and Biosystems Engineering, South Dakota State University, Brookings, SD, USA; [b]Department of Electrical Engineering and Computer Science, South Dakota State University, Brookings, SD, USA

ABSTRACT

The aim of this study is to develop and characterize an activated biochar-based polymer composite for biosensors in smart food packaging. Biochar was made from corn stover and activated using the steam-activation method. The activated biochar (ABC) was synthesized with polylactic acid (PLA) by a solvent casting method. While ABC ranged from 85% to 50%, PLA content varied from 15% to 50% (w/w) in the polymer composite. The electrical conductivity of the developed ABC/PLA composite was measured through differential plus voltammetry (DPV) and cyclic voltammetry (CV) using a potentiostat. It was found that the current increased from 0.3 to 2.31 mA for CV and 0.16 to 1.02 mA for DPV when ABC contents changed from 50% to 85%. The tensile strength (TS) and Young 's modulus of the ABC/PLA composite film increased from 0.81 to 3.04 MPa and 56.31 to 102.69 MPa respectively when PLA contents increased from 15% to 50%. The biosensor was fabricated with 85% ABC/PLA-based composite using a drop-casting method. The resistance of the fabricated biosensor increased as the concentration of NH_3 increased over the range of 80 to 170 ppm.

ARTICLE HISTORY
Received 24 December 2020
Accepted 20 April 2021

KEYWORDS
Activated biochar; polymer; composite; polylactic acid; biosensor; smart packaging

Introduction

Over the last few decades, food scientists have been increasingly interested in developing a variety of food safety measures to serve the qualitative foods.[1] Particular interest in this regard is the development of a biosensor for smart food packaging, which could be a rapid, concise, reliable, cost-effective and nondestructive tool.[2,3] Smart food packaging is an upgraded packaging nanotechnology that enables a communication between consumers and packaged foods about the condition of the packaged product.[4] Some film indicators have been developed for smart food packaging, such as pH-sensitive nanocomposite,[5] polyamide composite film,[6] time-temperature-based indicator (TTI)[7] and Al-doped ZnO composite film.[8] However, most of these film indicators contain costly raw sensing ingredients,[9] impair processing difficulties,[10] and cannot be reused.[11] Biosensors are a new alternative method, as they can easily detect the analytes within a second,[12] are easy to use and do not need complicated sampling steps.[13]

The market of petroleum-based polymers such as polystyrene, polypropylene, polyvinyl chloride, etc., has expanded in the twentieth century due to construction, automation and packaging industries.[14] However, the petroleum-based polymers have some drawbacks, such as they are non-biodegradable; affect the environment after their burning; and impede land fertility in

CONTACT Lin Wei lin.wei@sdstate.edu Department of Agricultural and Biosystems Engineering, South Dakota State University, Brookings, SD, USA.

contact with soil.[15] Therefore, we need to reduce our reliance on petroleum-based polymers to mitigate the environmental crisis. There is a growing interest in research into environmentally friendly and biodegradable polymers, which have become a popular topic worldwide.[16] Of the biodegradable polymers, polylactic acid (PLA) is the most widely used eco-friendly polymer and occupies an important position in the market due to its biomedical, tissue engineering, food service wares and packaging film application.[17,18] Despite having suitable packaging related properties, PLA has some drawbacks also, such as brittleness,[19] poor processability, poor heat resistance [20,21] and low toughness.[22] To mitigate these problems, PLA can be mixed with different carbon components, that is, multi-walled carbon nanotube, graphene, activated carbon and biochar that comes with some benefits as they improve the mechanical, thermal and electrical properties.[23,24] Among the carbon items, biochar from corn stover is an inexpensive and renewable source materials. In this study, PLA has been considered for using with biochar for biosensor construction as a cost-effective and rapid sensor tool for smart food packaging.

Biochar is one of the richly carbonaceous items which is derived from anaerobic thermal decomposition of biomass feedstocks such as agricultural crops, wood, leaves, woodchips, and waste.[25,26] For years, it has been using as pollutant adsorbent.[27] Biochar has some advantages over other carbon items (single or multi carbon nanotubes, activated carbon and graphene), such as it bears high specific surface area; has a highly porous structure, good stability, and cost-effectiveness.[28–30] The conventional biochar is normally in millimeter-scale and not electrically conductive; therefore, it shows the difficulty in constructing biosensors.[31] Rather, with its activation, the biochar with size reduced to nano or micro-scale can create electrical conductivity and formulate the biosensor and biosensing composite. In addition, after activation, biochar can obtain a greater surface area and more adsorption sites for target analytes, and promote rapid electron transfer during sensing and biosensing.[30]

In this study, PLA has been imparted with activated biochar to produce the conductive composite and this composite was used to develop a biosensor for smart food packaging. To the best of our knowledge, this is the first study on the development of activated biochar-based composite for biosensors and no research has been performed yet on its use and characterization for smart food packaging. Therefore, the goal of this work is to develop the composite materials using activated biochar and PLA blends and characterize their physical and electrical properties for biosensors. The objectives of this study are to 1) activate the biochar from corn stover and characterize their physical and electrical properties; 2) characterize the activated biochar-based composites for biosensor development; and 3) characterize the developed biosensor depending on the ammonia concentrations.

Materials and methods

Materials

Polylactic acid (PLA) employed in this research work was procured from Sigma Aldrich (St. Louis, MO, USA). The density, melting point and glass transition temperature of PLA were 1.24 g/cm^3, 160 °C and 57.8 °C, respectively. The potassium chloride (KCl) with purity with 99.0%) and potassium ferrocyanide (K_4 [Fe (CN) $_6$]) were procured from Sigma Aldrich (St. Louis, MO, USA) and used for biosensor characterization. Phosphate-buffered saline (PBS) was purchased from Thermo Fisher Scientific and made by combining with purified water at 10% (v/v).

Preparation of biochar from corn stover

Biochar was derived from corn stover, locally accumulated from corn fields at Brookings, SD 57007, using the accurate control pyrolysis (ACP) method developed by Dr. Lin Wei.[32] The

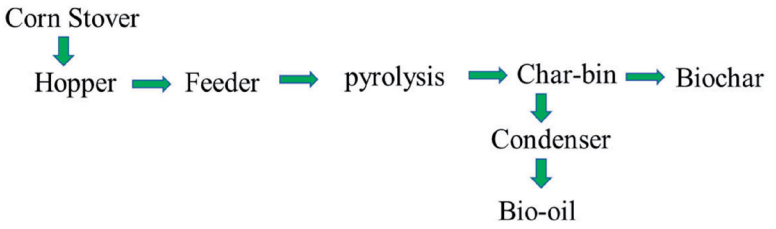

Figure 1. Biochar preparation from corn stover using accurate control pyrolysis (ACP) reactor system.

corn stover was weighed first and transferred into the hopper of ACP reactor (Figure (1)). Second, the corn stover inside the hopper was fed via a feeder and transferred in the reaction chamber of the ACP reactor, where corn stover was pyrolyzed to a vapor phase containing organic compounds and water vapor. The heat conduction within the reaction chamber was occurred and made the pyrolysis process easier and speedier. After pyrolysis, the hard biochar was produced and moved from the reaction chamber to a char bin chamber where the solid biochar particles were isolated from the vapor streams. Afterwards, the vapor streams were exited and condensed into liquid bio-oil in a condenser. The biochar particles were collected from char bin and used for activation using steam-activation method.

Biochar activation using steam-activation method

To activate the biochar sample, a steam-activation system was designed and fabricated for the activation process. The configuration of this system is shown as Figure 2, which consists of: (1) high-temperature steam chamber; (2) N_2 gas flow chamber; (3) tubular reactor and (4) gas outlet line. First, the biochar particles obtained from corn stover were finely milled using the omni mixer homogenizer (Waterbury, Ct., USA). Thereafter, the fine biochar particles were suspended in distilled water and centrifuged at 5000 rpm for 5 min. Following this, the supernatants containing biochar were collected and dried in an oven at 100 °C overnight. Second, 2 grams of dried biochar sample was taken into a tubular reactor (3). Then, the tubular reactor was placed into the reactor chamber. Thereafter, N_2 gas with 200 cm/min from the gas chamber (1) and steam with 2 mL/min via steam chamber (2) were continuously flowed to the tubular reactor during the activation process. Biochar activation was monitored at different temperatures, from 600 to 1000 °C of the tubular reactor, for 1 h. It is noted that this transmitted steam to tubular reactor allowed the activation of the biochar particles and the flowed N_2 gas evacuated the steam from the tubular reactor through the outlet line. After that, tubular reactor with activated biochar was taken out from reaction chamber and the activated biochar (ABC) was collected for further analysis.

$$\text{Biochar} + \text{Steam} \xrightarrow{800^{\circ}C} \text{Activated biochar} + \text{Carbon di} - \text{oxide} \quad (1)$$

Characterized analysis of activated biochar (ABC)

Raman spectroscopy analysis

Raman spectroscopy is one of the spectroscopic techniques used to determine chemical and structural properties of sample molecules. To identify the structural characteristics of ABC, ABCs generated at different temperatures were analyzed using Raman spectroscopy (LabRAM HR, HORIBA Scientific). A linearly polarized laser light with a wavelength of $\lambda = 532$ nm was considered by a diffraction-limiting spot size (0.61 λ/NA). The wavenumber range was taken between 1000 and 2000 cm^{-1} for IR spectrums.

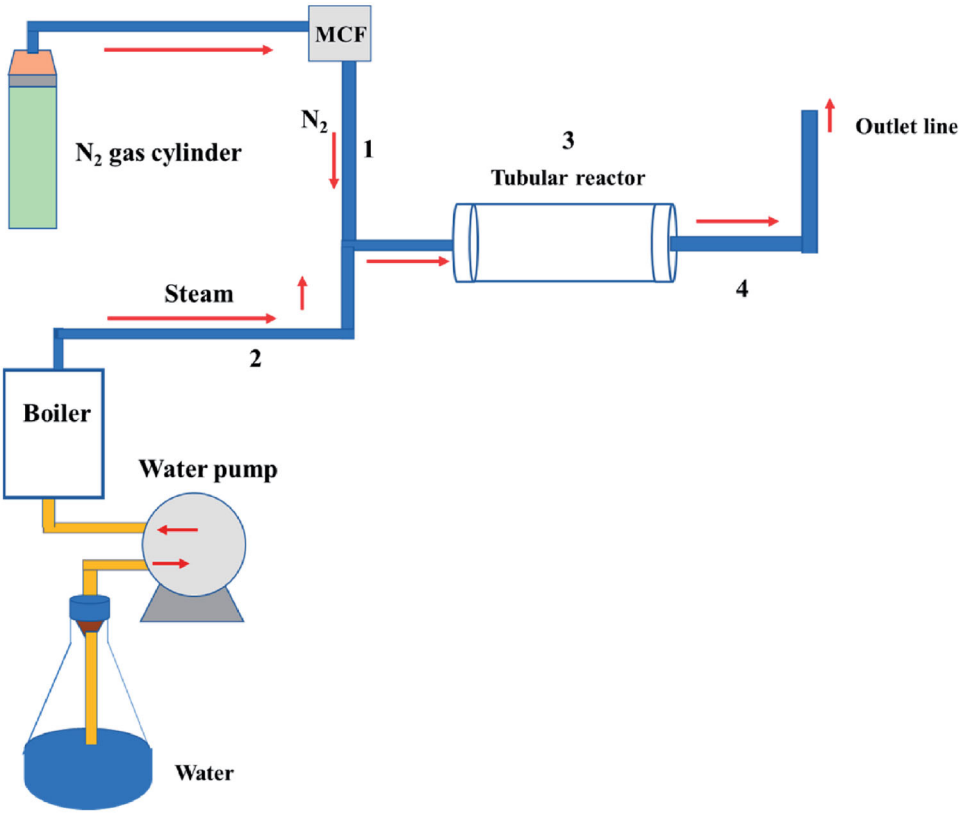

Figure 2. Configuration of biochar activation followed by the steam-activation method.

Brunauer–Emmett–Teller (BET) analysis

The surface area and pore size distributed in the activated biochar sample were evaluated using a Surface Area and Porosity Analyzer (Micromeritics ASAP 2020, USA) which was automated with the nitrogen gas sorption system. For this test, the activated biochar samples were degassed under vacuum at 110 °C overnight to remove residual moisture prior to nitrogen gas adsorption. The adsorption curves of nitrogen gas obtained for each biochar sample was used to compute the specific BET surface area, and the pore grades.

Scanning electron microscopic analysis

Microstructural analysis of ABCs has been observed by scanning electron microscopy (SEM) (Hitachi-S-3400, filament-based SEM, MO, US). For ABCs, the ABCs samples were first smeared on the SEM observation template with 2 mm × 2 mm. Afterwards, the surfaces of ABC were observed at a working distance of 10 mm with a magnification of 1500× under 10 kV electrical voltage.

Development of biosensor for ABCs characterization

The biosensor consisted of Au-electrodes upon alumina substrate and was used as the primary sensing platform. To construct the biosensor platform, Au-electrodes were threaded over the alumina substrate using electron-beam evaporator (Case Western Reserve University, Ohio, USA). Afterwards, the Au-electrodes were dried using N_2 and kept into vacuum chamber after electrical testing. The electrical conductivity of the Au-deposited platform was also tested to ensure that

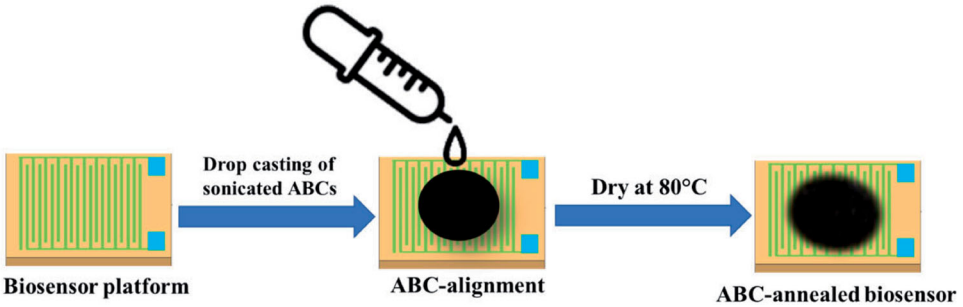

Figure 3. Schematic illustration of biosensor fabrication process using drop casting.

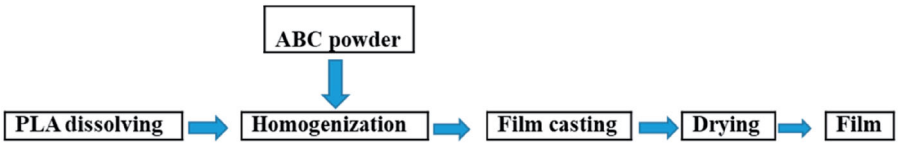

Figure 4. Stepwise fabrication process of ABC/PLA composite film.

the Au-electrodes were able to work effectively. The biosensor fabrication was performed according to a drop casting method (Figure (3)).[13,33,34] First, ABC samples activated at 600–1000 °C were individually sonicated for 1 h at the concentration of 1 mg/mL in DMF (N, N-dimethylformamide). Afterwards, an aliquot of 15 µL of sonicated ABC suspensions was dropped onto the biosensor surface for alignment. The aligned biosensor was annealed at 80 °C for 10 min in a dryer to bond the ABC residuals to the electrode surface. Following this step, the annealed electrode was rinsed with deionized water to elute the unbound ABCs from the biosensor surface. After following this step, linear sweep voltammetry (LSV) measurements were performed from 0.0 to 0.1 V for each measurement to estimate electrical conductivity of ABCs.

Preparation of ABC/PLA composite film

Composite film is a type of film which is a flat, thin, and dry form of composite. A schematic diagram of the fabrication of ABC/PLA composite film has been shown in Figure 4. This composite film was synthesized using a solvent casting method. First, different ABC/PLA labels (w/w) were prepared, which were 85% (85% ABC with 15% PLA), 70% (70% ABC with 30% PLA) and 50% (50% ABC with 50% PLA). Next, ABC/PLA mixtures were homogenized for 15 min with a handheld homogenizer (PRO scientific, USA). After homogenization, the homogenized mixture was poured into the stainless-steel petri-dish and dried at room temperature (~20 °C) for at least 1 day. The dried films were peeled from the stainless-steel petri-dish and then conditioned with 50–60% relative humidity (RH). ABC/PLA films were prepared in triplicate for film characterization. The thickness of the film was measured using a handheld micrometer (Esslinger, MN, USA).

Characterized analysis of ABC/PLA composite film

Mechanical analysis

Mechanical analysis is a technique which is used to measure the tensile properties of composite film. ABC/PLA composite film was mechanically analyzed by following the method developed previously.[9] A texture analyzer fitted with Texture Exponent 32 software (Texture Technologies Corp., Scarsdale, NY, USA) was used to compute tensile force and deformation. Before the test,

the film strips had been cut consistently to 50 mm long and 20 mm wide. The crosshead speed was set to 60 mm/min. Tensile strength (TS), strain, and Young's modules were determined based on the strength and deformation data recorded by the following equation.

$$\text{TS} = \frac{\text{Maximum applied force}}{\text{Film thickness} \times \text{Film width}} \tag{2}$$

$$\text{Strain} = \frac{\text{Elongation}}{\text{Original leanth of film}} \tag{3}$$

$$\text{Young's modulus} = \frac{\text{TS}}{\text{Strain}} \tag{4}$$

Thermogravimetric analysis

Thermal analysis of ABC/PLA composite film were performed by thermogravimetric analyzer (TGA) (Q5000 SA, TA Instruments, USA). For this test, 3 mg of each ABC/PLA film was placed directly in a hermetically sealed pan. Afterwards, the specimens were subsequently heated in a 20–400 °C range under a nitrogen atmosphere with a heating rate of 10 °C.min^{-1} and a gas flow rate of 20 mL.min^{-1}.

Electrical analysis of ABC/PLA composite

Cyclic voltammetry (CV) and differential plus voltammetry (DPV) were used for characterizing ABC/PLA composites prepared by film casting process. For this test, a redox solution, containing 2.5 mmol L^{-1} [Fe (CN)6]$^{3-}$ and 0.1 mol L^{-1} KCl prepared in PBS buffer (pH 7.4, 0.1 M), was used. Three electrodes were considered as a working electrode of 2 mm diameter, Ag/AgCl of 3.0 mol^{-1} KCl as the reference electrode and a platinum wire as a counter electrode. ABC/PLA film suspension was added sequentially to the sensing surface of working electrode and was dried overnight at room temperature. After that, the fabricated working electrode with reference and counter electrode was dipped in redox solution. After the scans, the CV and DPV signals were obtained while the scan rate of 100 mV^{-1} was sustained and the voltage was between +600 mV and −200 mV.

ABC/PLA-based biosensor development for ammonia (NH_3) detection

Figure 5 shows a schematic diagram of the experimental setup for measuring the biosensor's response with regard to standard NH_3 gas balanced with nitrogen (N_2). This system was formed using hammond gas chamber (188 mm × 120 mm× 50 mm) including electrical connections lined with the 85% ABC/PLA-based biosensor and NH_3 gas tank. The desired concentrations of NH_3 flowed into hammond gas chamber were maintained by computer-based gas control system.

In this study, linear sweep voltammetry (LSV) analysis was performed at each step using a potentiostat (DY2013, Digi-Ivy, Inc., Austin, USA). The slope of the current/voltage (I/V) between 0.0 V and 0.12 V was estimated using linear regression analysis. The sensitivity of the biosensor toward the exposure of NH_3 was calculated as:

$$\text{Sensitivity} = (R_1 - R_0)/R_1 \tag{5}$$

where, R_0 = the resistance of the biosensor without gas (base resistance) and R_1 = the resistance of the biosensor when exposed to gas.

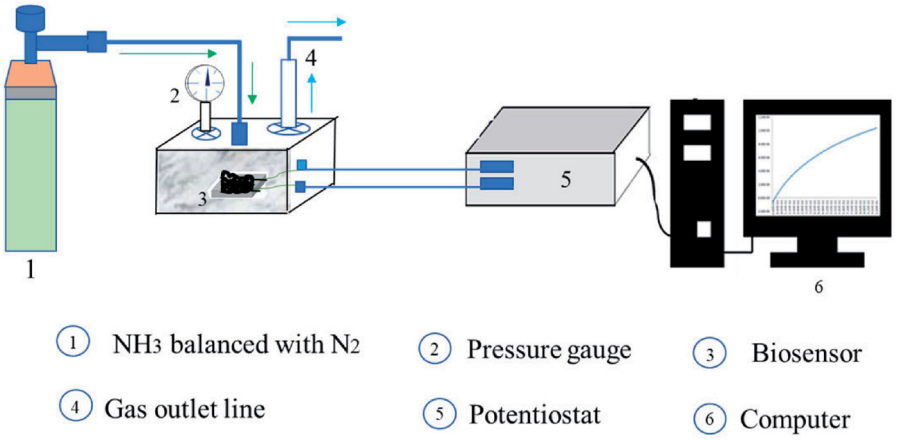

Figure 5. Schematic diagram of the experimental set-up for measuring biosensor response to NH_3.

Statistical analysis

The statistical data analysis was carried out by one-way analysis of variance (ANOVA) and significant analysis of the data was performed by Tukey test with considering a defined significance level of $p < 0.05$.

Results and discussion

Characterization of activated biochar (ABC)

Physical properties of ABC sample

Raman spectroscopy is a useful technique that is used to characterize and understand the materials properties, including molecular and chemical structure, crystallinity, phase and molecular interaction.[26] In order to generate highly conductive biochar, biochar was thermally activated for developing biosensor for smart food packaging application. After activation with different temperature, the biochar was further characterized using Raman spectroscopy to illustrate the physical features. The Raman spectrums of ABC for different temperature have been displayed in Figure 6. In this Figure 6(A), two highly peak bands were inspected corresponding to G band at 1590 cm^{-1} and D band at 1380 cm^{-1}. The D band correlates to the vibration of defective carbon or sp^3 carbon atoms in the disordered graphite structure, while G band conforms to the in-plane vibration of sp^2 carbon atoms in the two dimensional hexagonal lattice of graphene.[35,36] The intensity ratio of D to G (I_D/I_G) was found to 0.81, 0.61, 0.94, 0.89 and 0.87 for 600 °C, 700 °C, 800 °C, 900 °C and 1000 °C respectively. It is clearly seen that the intensity ratio of I_D/I_G for ABC/800 °C was higher as 0.94 compared to the other intensity ratio (I_D/I_G) for other activation temperatures, indicating more vacancy defects were produced in ABC at 800 °C.[26] Thus, it can be said that temperature has an effect for biochar activation.

The surface area and pore volume upon the biochar are the crucial factors when biochar is considered for biosensor construction for gas absorption and as the potential filler for polymeric composite preparation.[37] The extensive surface area and internal pore structure of biochar can contribute to high absorption capability and serve a good mechanical interlocking between filler and matrix.[38] BET surface area and pore volume of biochar activated at different temperature has been displayed in Figure 6(B). As seen in Figure 6(B), BET surface area along with the pore volume of biochar at 800 °C was significantly higher, as 825.89 m^2/g and 0.21 cm^3/g respectively, compared to the other biochar sample activated at 600 °C, 700 °C 900 °C and 1000 °C. This

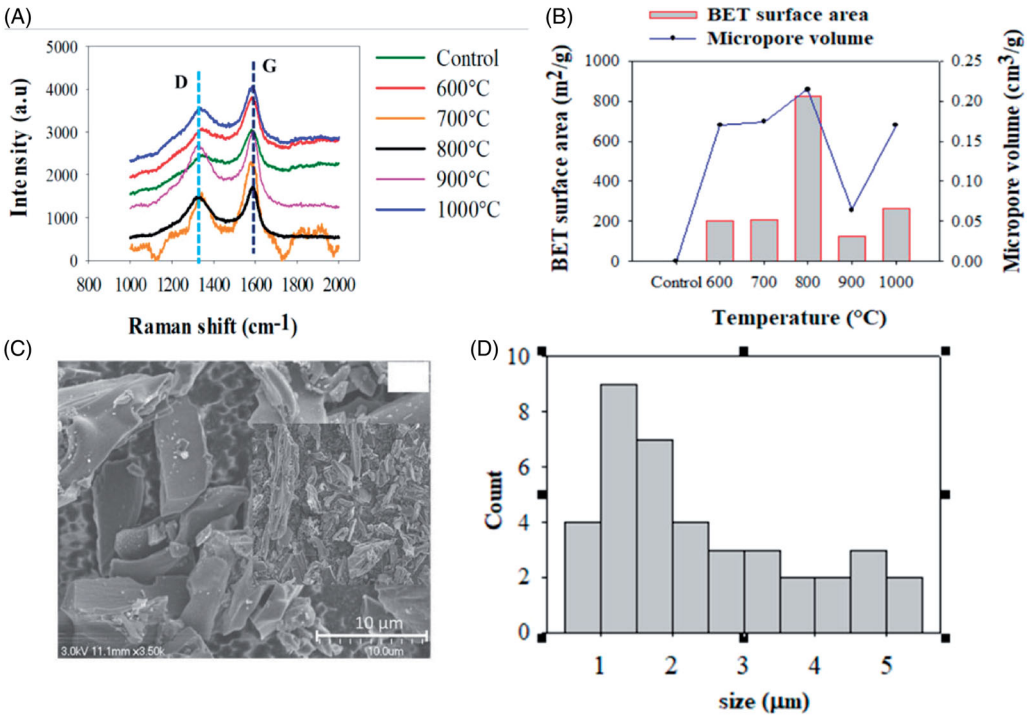

Figure 6. Characterization of ABCs. (A) Raman spectrums of the ABCs with different temperature range (600–1000 °C); (B) BET analysis of ABCs; (C) SEM images of ABC/800 °C; and (D) Histogram of ABC/800 °C. Control sample denotes biochar sample without thermal activation.

increased surface area and pore volume might be occurred because of the removal of carbon mass and volatile matters from biochar surface during activation process.[39] Greater surface area is desirable because it aids in absorbing gas and molecules to a greater extent. However, biochar activated at 600 °C, 700 °C, 900 °C and 1000 °C showed lower BET surface area. It might be volatile matters were not effectively removed from biochar surface and not effectively activated at those temperature. In addition, no surface area was detected for control biochar sample due to a negative isotherm due to its releasing N_2 gas.

In the SEM analysis, it is seen in Figure 6(C), the ABC/800 °C had irregular and heterogeneous shape. The size distribution of the ABC/800 °C was determined using Java-based image processing program (ImageJ developer, USA). The mean size distribution of ABC/800 °C was illustrated in Figure 6(D). Approximately 41.01% of ABC/800 °C is 1-2 µm, 17.94% is 2-3 µm, and 25.62% is 3-4 µm, the average particle size is 3 µm, indicating that micro-size ABC particles were successfully produced.

Electrical analysis of ABC sample

To investigate the electrical conductivity of the ABCs, biosensor was developed with ABC/600 °C, ABC/700 °C, ABC/800 °C, ABC/900 °C and ABC/1000 °C and characterized their electrical properties. As can be seen in Figure 7(A), the current obtained at ABC/800 °C was much higher than those of other biosensors made with ABC/700 °C, ABC/900 °C and ABC/1000 °C. No current was detected for the biosensor prepared by ABC/600 °C sample. This indicates that the biochar was slightly activated at 700 °C, 900 °C and 1000 °C but not electrically properly activated at 600 °C. In Figure 7(B), Nyquist current curves obtained by linear sweep voltammetry (LSV) were presented and found that current at ABC/800 °C was significantly higher compared to current at

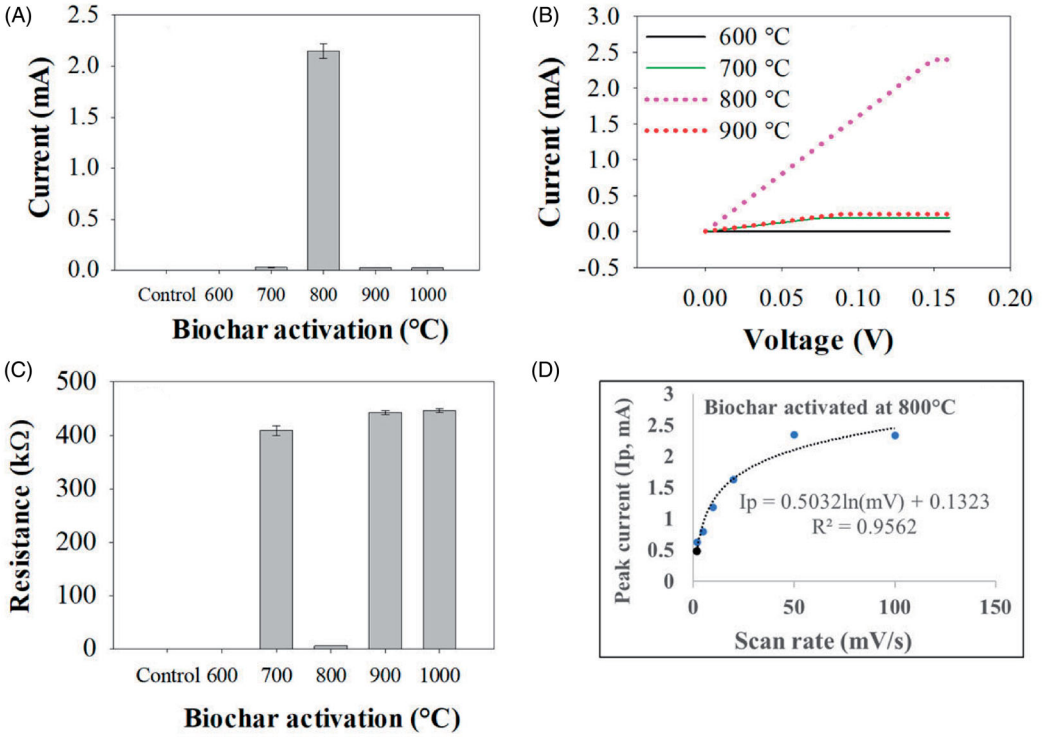

Figure 7. Electrochemical analysis of ABCs. (A) Current of ABCs; (B) Nyquist current curves obtained by linear sweep voltammetry; (C) Resistance of ABCs; and (D) Plot of peak current (Ip) versus different potential scan rates. Control sample denotes biochar sample without thermal activation.

ABC/700 °C and ABC/900 °C, which confirmed that ABC/800 °C sample is consisted of highly conductive ABCs particles. Since the biosensor made with ABC/600 °C did not show electrical conductivity, which ensured that ABC activation was not perfect at less than 700 °C, though the electrical conductivity at 700 °C, 900 °C and 1000 °C was much lesser. As can be seen in Figure 7(C), the resistance of the biosensor made with ABC/800 °C was much lower compared to the biosensor made with ABC/700 °C, ABC/900 °C and ABC/1000 °C, which means that the larger electron transfer property at ABC/800 °C was achieved. These conductivity results of ABCs confirmed that the physical and chemical properties of ABCs were changed under temperature treatment during activation.[26] To further characterize ABC/800 °C sample, linearity plot of peak current (Ip) vs. different potential scan rates (mV/s) was constructed throughout the CV cycle and found that there is a good co-relation between Ip and scan rates (Figure 7(D)). In previous studies, the non-conductive carbon of cellulose and lignin was converted to conductive graphene, while SP^3 carbons were transformed into SP^2 carbon.[31] Due to its high electrical conductivity, ABC/800 °C sample was considered for the preparation of biosensing composites in this study.

Characterization of ABC/PLA composite

Physical properties of ABC/PLA composite film

ABC/PLA composite films containing 85-50% of ABC/800 °C (w/w) corresponding to 15-50% PLA (w/w) were shown in Figure 8(a). The surface morphological features of the films were evaluated using SEM to observe surface layers of the PLA/ABC film, as seen in Figure 8(b). The composite film was not transparent and had a black color in its final appearance because it contained biochar particles. The average weight of each film was measured as ~500 mg and the thickness

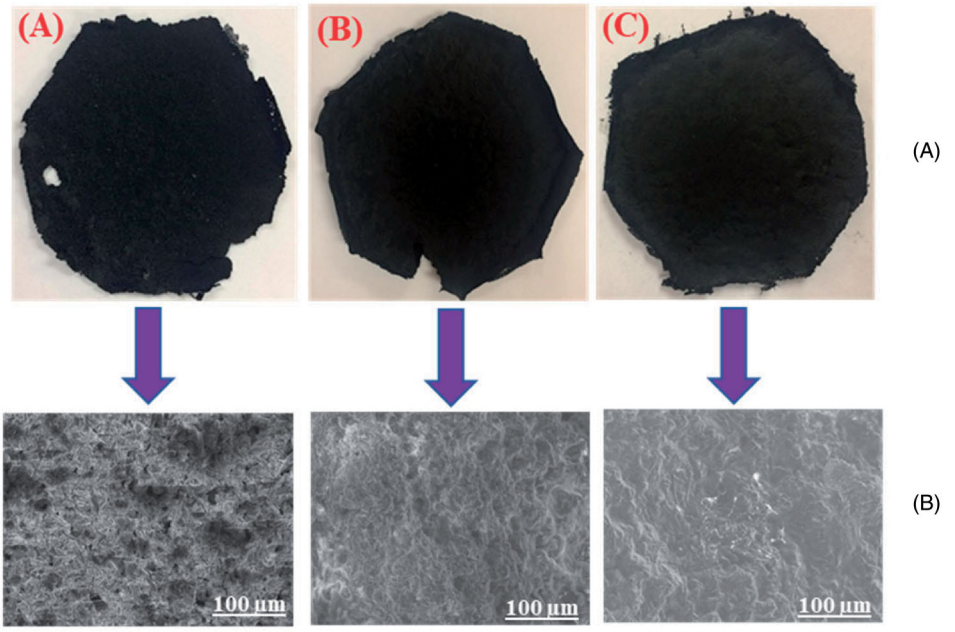

Figure 8. Physical properties of ABC/PLA films. **A: Left to right**: 85% ABC/PLA film; 70% ABC/PLA film; 50% ABC/PLA film; **B: left to right:** SEM micrographs of 85% ABC/PLA film; 70% ABC/PLA film; 50% ABC/PLA film.

varied between 0.35–0.37 mm. These films were homogeneous and easy to use by hand. SEM micrographs of the film showed that increasing the PLA content to the film formed a relatively dense and hard surface to the final appearance compared to the decreasing PLA contents to the film (Figure 8(b)). Therefore, 50% ABC/PLA film showed the greatest adhesion at the interface between ABC and PLA compared to 85% ABC/PLA film. It was seen in SEM (Figure 8(b)) that the 85% ABC/PLA film had a large number of micropores on their film appearance, which could be a clue for absorbing gas or molecules inside the micro-pore volumes.

To investigate the deeper microstructure of ABC/PLA composite film, SEM analysis with 10 µm scale bars was performed. The size distribution of native ABC and PLA particles in the film were seen in the SEM micrographs. Th random orientations of ABC combined with lesser PLA contents were seen in 85% ABC/PLA film (Figure 9(A)). The compact binding of ABC with increasing PLA was formed in 70% ABC/PLA film (Figure 9(B)). The abundant amounts of PLA were inspected in 50% ABC/PLA film and ABCs were not clearly observed in 50% ABC/PLA film (Figure 9(C)). This is because a compact and strongest bond was formed between ABC and PLA in 50% ABC/PLA film. This intricate structure of 50% ABC/PLA film indicates that the constituent elements of PLA and ABC may improve the mechanical properties of ABC/PLA film.

Mechanical properties of ABC/PLA composite

Mechanical properties of ABC/PLA composite film were determined to examine the tensile properties of the film with respect to applied force. As can be seen in Figure 10, when the ABC contents in the ABC/PLA film decreased from 85% to 50% and PLA contents alternatively increased in the ABC/PLA film from 15% to 50%, the tensile properties, including tensile strength (TS), Young's modulus and strain increased at the same time. This increase of tensile properties with increasing PLA and decreasing ABC is one of the reasons for rising the tensile properties of ABC/PLA film. This increasing PLA contents to the film may allow the film to withstand the normal stress faced during the shipment, handling and transportation of foods.[40] The other possible

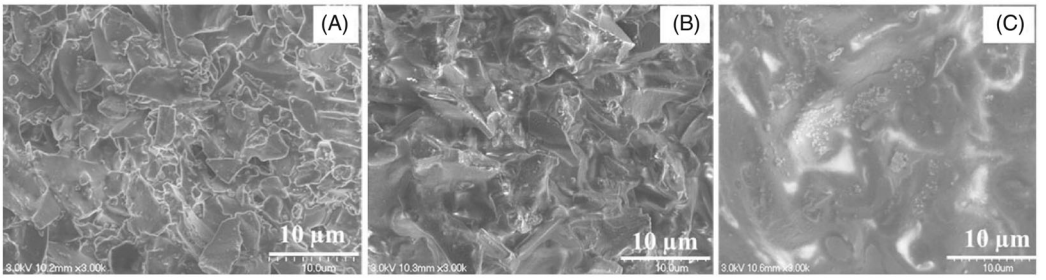

Figure 9. SEM micrographs of ABC/PLA film. (A) 85% ABC/PLA film; (B) 70% ABC/PLA film; (C) 50% ABC/PLA film.

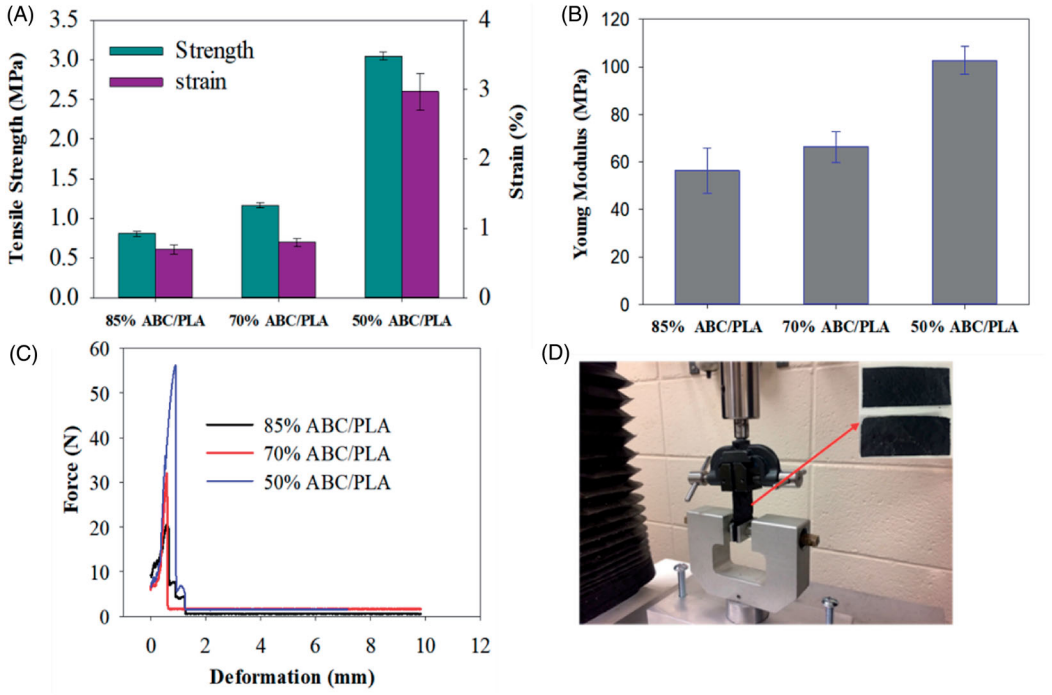

Figure 10. Tensile properties of ABC/PLA composite film. (A) Tensile strength and strain; (B) Young's modulus; (C) force vs deformation of 85% to 50% ABC/PLA composite film; and (D) scheme of tensile testing.

reason of increasing tensile properties of the film is related to interfacial interaction of increasing PLA with decreasing ABC, because PLA as the plasticizer agent which may strictly bind ABCs in the ABC/PLA film.[41] Therefore, it permits the higher tensile force during the film deformation; and resulted in an increase in tensile strength. Compared to the films, 50% ABC/PLA film has higher tensile properties ($p < 0.05$).

Thermal properties of ABC/PLA film

TGA analysis was performed to understand the thermal behavior of ABC/PLA composite film in the temperature range of 20–500 °C under nitrogen gas (N_2) conditions, as shown in Figure (11). The thermal decomposition stage of the ABC/PLA composite film is divided into three main consecutive regions, and these three regions occur continuously. First, the initial weight loss of ABC/PLA composites occurred at 20–200 °C. At this phase, it is thought that the physically unbound water molecules from ABC/PLA composite were evaporated. Secondly, between 290–430 °C, the

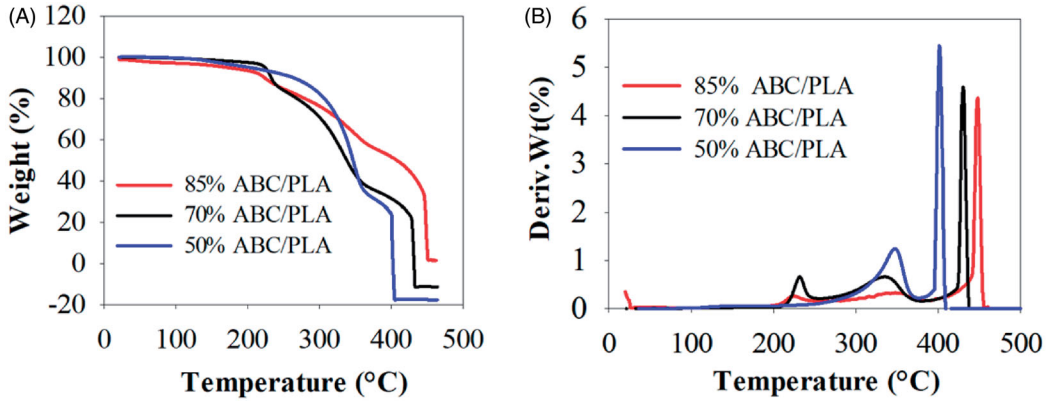

Figure 11. TGA spectra of ABC/PLA composite film under nitrogen (N_2) condition. (A) TGA curve for different ABC/PLA composite films; (B) Differential of TGA (DTGA) curves of different ABC/PLA composite films.

weight of the ABC/PLA composite is significantly reduced. At this phase, the 50% ABC/PLA-based composite was significantly degraded between 200 and 400 °C compared to the 70% and 85% ABC/PLA-based composite film. At the same time, compared with the content of other composites, 85% ABC/PLA composite has less thermally degraded because of containing less amount of PLA. The third stage of all these composites occurred at 400–450 °C. At this stage, the residual organic matter was oxidized or carbonized, and the carbonized residue remains in the aluminum pan. Similar thermal stability phenomena has been examined in previous work, in which the weight loss of silver integrated composite film decreased as the metal nanoparticles into the film increased.[42]

Electrical properties of ABC/PLA composite

Biosensor developed with 85 to 50% of ABC/PLA-based composite was characterized electrically using cyclic (CV) and differential plus (DPV) voltammetry analysis. According to the Figure 12(A), while ABC contents in the ABC/PLA composite rose from 50% to 85%, the CV current increased from 0.32 mA to 2.3 mA. This increase of peak current implied that the composite with increasing ABC and decreasing PLA employed a greater surface of the gold working electrode and effectively transferred electrons in the $[Fe\ (CN)_6]^{3-}$ solution. In the similar manner, as shown in Figure 12(B), peak current obtained by DPV increased as ABC concentrations into the ABC/PLA composite increased from 50% to 85%. This increase in DPV current demonstrated that a large amount of ABC promotes the dispersion of redox ions to the gold working electrode surface, thus leading to a rise in voltammetry current. In previous studies, a similar increase of current was noticed, while the working electrode was fabricated with activated carbon-based composites from lower to higher concentration.[11,33,43] The peak current of CV and DPV was presented in Figure 12(C). It is seen that peak current increased as the ABC in the PLA/ABC composite increased. Current density for different ABC/PLA composite film has been displayed in Figure 12(D). 85% ABC/PLA-based composite showed higher current density with higher performance compared to 70% and 50% ABC/PLA-based composite. To validate the advantages of the PLA/ABC composite, CV current was characterized with different scan rates from 5 to 100 mV/s. The peak current rose as the scan rate increased from 2 to 100 mV/s, which revealed that the peak current of CV has a good linear relationship with the increase in scan rate. Though 50% ABC/PLA composite has high tensile properties, but it possessed low thermal stability and poor electrical conductivity. Besides, 70% ABC/PLA composite has poor electrical conductivity

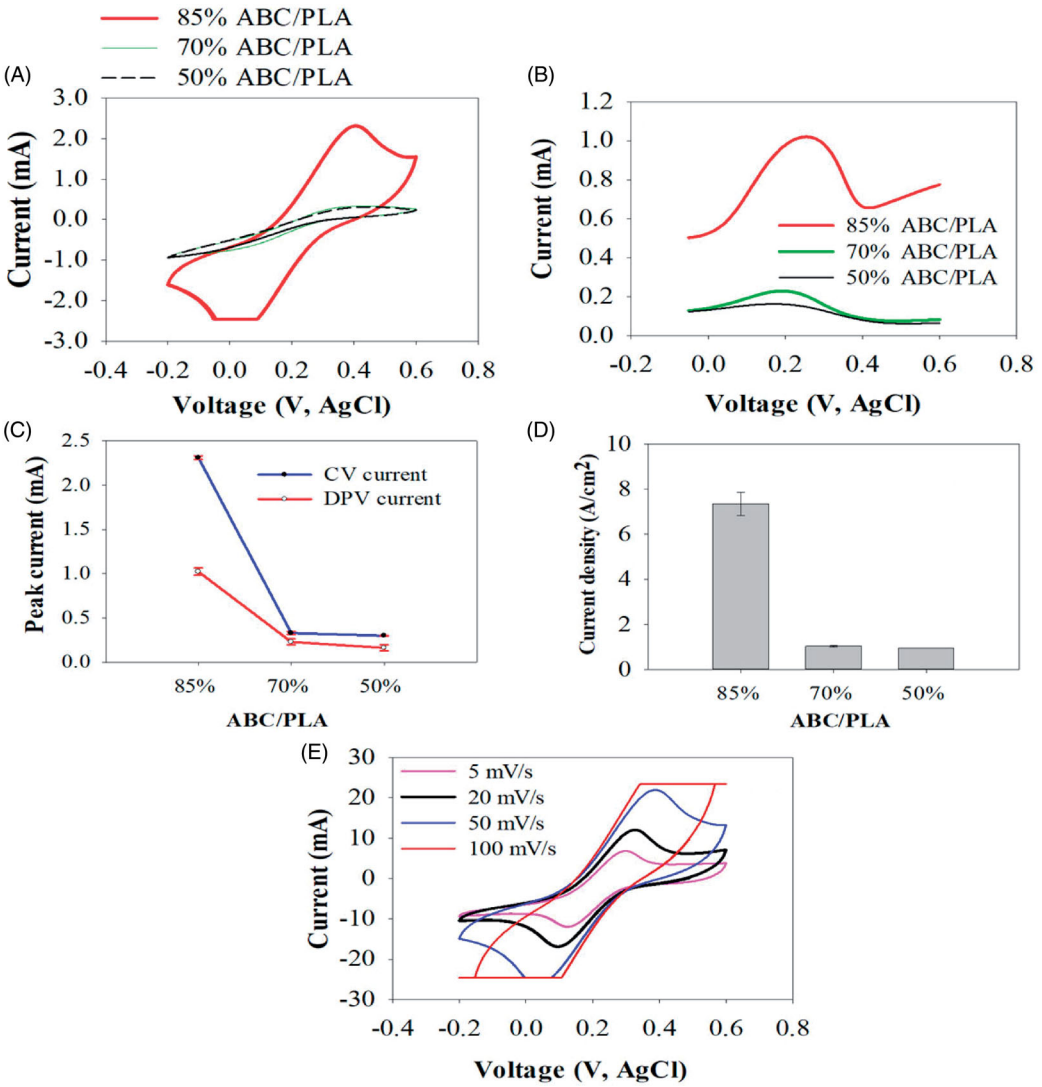

Figure 12. Electrical analysis of 85%-50% ABC/PLA composite. (A) Cyclic voltammogram (CV); (B) differential plus voltammogram (DPV); (C) peak currents of ABC/PLA; (D) current density of ABC/PLA; and (E) cyclic voltammogram with different scan rates (5 to 100 mV/s).

and low thermal stability. Because of this, 85% ABC/PLA composite containing higher electrical conductivity is suitable for biosensor development for smart food packaging.

ABC/PLA-based biosensor for ammonia (NH3) detection

The biosensor fabricated with 85% ABC/PLA-based composite was examined with regard to different standard NH_3 concentrations to understand how the developed biosensor is related to the adsorption mechanism. Ammonia (NH_3) is one of the popular components of volatile gas that is emitted with other volatile materials, including esters, ketones, alcohol and aldehydes during beef spoilage[44–46] and wanted to check in this test how the 85% ABC/PLA biosensor behaves with the standard NH_3 specimens. The resistance (R) values of the 85% PLA/ABC-based biosensor when responding to the selected concentration of NH_3 have been presented in the Figure 13(A).

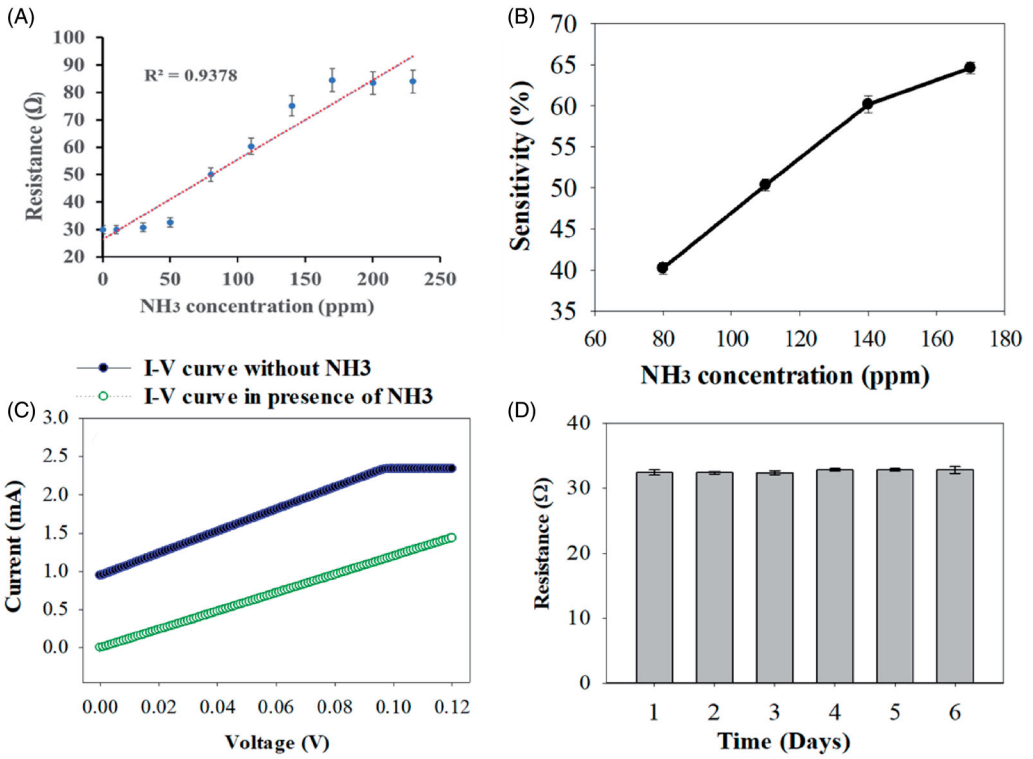

Figure 13. (A) Resistance response of 85% ABC/PLA-based biosensor to NH_3 concentrations (5 ppm to 230 ppm); (B) Sensitivity of the biosensor to NH_3 gas (80-170 ppm); (C) Comparison of I-V data of 85% ABC/PLA-based biosensor in presence and absence of NH3 gas (~110 ppm); (D) Stability of the biosensor for fixed NH_3 concentration (50 ppm).

It is seen that when the concentrations of NH_3 increased, the R values of the biosensor also rose. This is a typical characteristic of carbon-based biosensor (single or multi-walled carbon) which reacts to increasing concentration of the NH_3.[47] The reason of increasing resistance might be related to the hole depletion of the sensing material; thus, it influences the conductivity of the biosensor. In addition, activated biochar has a large surface area (~825 m^2/g) which might be enabled the biosensor to absorb NH_3 gas in its micro-pore surfaces. However, the R values were not significant at a concentration of 0-80 ppm ($p > 0.05$). The significant linear range of R was seen between 80 and 170 ppm, and then no significant variation in the R values were inspected. The lack of linear increase in R values higher than 170 ppm concentration might be attributed to the fact that biosensor was fully saturated with the NH_3 gas concentration. The regression coefficient (R^2) value of the 85% ABC/PLA-based biosensor from the linear regression line was calculated to be 0.9378. The optimum concentration range of NH_3 for the 85% ABC/PLA-based biosensor was between 80-170 ppm; therefore, the limit of detection (LOD) of the 85% ABC/PLA-based biosensor was determined to be 80 ppm.

The sensitivity of 85% ABC/PLA-based biosensor was determined at the different concentrations of NH_3 gas from 80 to 170 ppm (~20 °C) and displayed in Figure 13(B). The dependence of sensitivity on the NH_3 in this range was linear. Nyquist curves for determining NH_3-sensing using 85% ABC/PLA-based biosensor have been shown in Figure 13(C). The data show the current-voltage (I-V) relationship in presence and absence of NH_3 gas. As can be seen in I-V curve, biosensor exposed to NH_3 revealed lower current compared to unexposed biosensor. Stability of the biosensor was also tested to a fixed NH_3 concentration (~50 ppm) over the 6 days. It is seen that resistance of the biosensor did not reveal the

significant fluctuation over the 6 days period, which implies that biosensor possessed good stability (Figure 13(D)).

Conclusions

In this study, biochar was activated at different temperatures and activated biochar (ABC) with higher conductivity was generated at 800 °C. ABC/800 °C served extensive surface area of 825.89 m^2/g and micropore volume of 0.21 cm^3/g for high-efficiency adsorption of the target analytes. The produced ABCs were efficient in producing ABC/PLA composite throughout film casting process. The ABC/PLA film microstructure obtained from SEM confirmed that 85% ABC/PLA film possessed multiple micropores on its surface and were aligned with PLA in the film formation. Compared to 70% and 85% ABC/PLA films, 50% ABC/PLA films are mechanically appropriate for rough use, but they have weak biosensing electrical properties that are not suitable for smart food packaging. The biosensor fabricated with 85% ABC/PLA-based composite resulted in higher electrical conductivity and revealed a sensitivity of ~40% at 80 ppm of NH_3 as a LOD.

Disclosure statement

The authors declare that there are no conflicts of interest.

Funding

This research was supported by the North Central Regional Sun Grant Center [Grant #: 3FG386], and the USDA NIFA program through the Hatch Project [No. 3AR676 and 3AH658] of the South Dakota Agricultural Experimental Station. Only the authors are responsible for the opinions expressed in this paper.

References

[1] Smigic, N., I. Djekic, I. Tomasevic, J. Miocinovic, and R. Gvozdenovic. 2012. Implication of food safety measures on microbiological quality of raw and pasteurized milk. *Food. Control.* 25:728–731.

[2] Kiryukhin, M. V., H. H. Lau, S. H. Goh, C. Teh, V. Korzh, and A. Sadovoy. 2018. A membrane film sensor with encapsulated fluorescent dyes towards express freshness monitoring of packaged food. *Talanta.* 182: 187–192. doi:10.1016/j.talanta.2018.01.085

[3] Kuswandi, B., and A. Nurfawaidi. 2017. On-package dual sensors label based on pH indicators for real-time monitoring of beef freshness. *Food. Control.* 82:91–100. doi:10.1016/j.foodcont.2017.06.028

[4] Schaefer, D., and Cheung, W. M. 2018. Smart packaging: opportunities and challenges. *Procedia CIRP.* 72: 1022–1027. doi:10.1016/j.procir.2018.03.240

[5] Zhang, H., A. Hou, K. Xie, and A. Gao. 2019. Smart color-changing paper packaging sensors with pH sensitive chromophores based on azo-anthraquinone reactive dyes. *Sen Actuat, B Chem.* 286:362–369. doi:10.1016/j.snb.2019.01.165

[6] He, X., and Y. Wang. 2020. Highly thermally conductive polyimide composite films with excellent thermal and electrical insulating properties. *Ind. Eng. Chem. Res.* 59:1925–1933. doi:10.1021/acs.iecr.9b05939

[7] Soon, J. M., and L. Manning. 2019. Developing anti-counterfeiting measures: the role of smart packaging. *Food. Res. Int.* 123:135–143. doi:10.1016/j.foodres.2019.04.049

[8] Rezek, J., P. Novák, J. Houška, A. D. Pajdarová, and T. Kozák. 2019. High-rate reactive high-power impulse magnetron sputtering of transparent conductive Al-doped ZnO thin films prepared at ambient temperature. *Thin. Solid. Films.* 679:35–41. doi:10.1016/j.tsf.2019.04.009

[9] Sobhan, A., K. Muthukumarappan, Z. Cen, and L. Wei. 2019. Characterization of nanocellulose and activated carbon nanocomposite films' biosensing properties for smart packaging. *Carbohydr. Polym.* 225: 115189. doi:10.1016/j.carbpol.2019.115189

[10] Jamróz, E., P. Kopel, L. Juszczak, A. Kawecka, Z. Bytesnikova, V. Milosavljević, M. Kucharek, M. Makarewicz, and V. Adam. 2018. Development and characterisation of furcellaran-gelatin films containing

SeNPs and AgNPs that have antimicrobial activity. *Food. Hydrocoll.* 83:9–16. doi:10.1016/j.foodhyd.2018.04.028

[11] Sobhan, A., J.-H. Oh, M.-K. Park, S. W. Kim, C. Park, and J. Lee. 2018. Assessment of peanut allergen ara h1 in processed foods using a SWCNTs-based nanobiosensor. *Biosci. Biotechnol. Biochem* 8451:1–9.

[12] Sobhan, A., J. Oh, and J. Lee. 2018. Rapid detection of ara h2 using single walled carbon nanotube based biosensor for peanut allergen control. *Amm.* 878:286–290. doi:10.4028/www.scientific.net/AMM.878.286

[13] Sobhan, A., J. H. Oh, M. K. Park, and J. Lee. 2020. Reusability of a single-walled carbon nanotube-based biosensor for detecting peanut allergens and *Y. enterocolitica*. *Microelectron. Eng.* 225:111281. doi:10.1016/j.mee.2020.111281

[14] Sánchez, C. 2020. Fungal potential for the degradation of petroleum-based polymers: an overview of macro- and microplastics biodegradation. *Biotechnol. Adv* 40:107501. doi:10.1016/j.biotechadv.2019.107501

[15] Li, Y., C. Jia, X. Zhang, Y. Jiang, M. Zhang, P. Lu, and H. Chen. 2018. Synthesis and performance of bio-based epoxy coated urea as controlled release fertilizer. *Prog. Org. Coatings.* 119:50–56. doi:10.1016/j.porgcoat.2018.02.013

[16] Doudin, K., S. Al-Malaika, H. H. Sheena, V. Tverezovskiy, and P. Fowler. 2016. New genre of antioxidants from renewable natural resources: Synthesis and characterisation of rosemary plant-derived antioxidants and their performance in polyolefins. *Polym. Degrad. Stab.* 130:126–134. doi:10.1016/j.polymdegradstab.2016.05.030

[17] Siripongpreda, T., K. Siralertmukul, and N. Rodthongkum. 2020. Colorimetric sensor and LDI-MS detection of biogenic amines in food spoilage based on porous PLA and graphene oxide. *Food. Chem.* 329:127165. doi:10.1016/j.foodchem.2020.127165

[18] Fortunati, E., I. Armentano, Q. Zhou, A. Iannoni, E. Saino, L. Visai, L. A. Berglund, and J. M. Kenny. 2012. Multifunctional bionanocomposite films of poly (lactic acid), cellulose nanocrystals and silver nanoparticles. *Carbohydr. Polym.* 87:1596–1605. doi:10.1016/j.carbpol.2011.09.066

[19] Palai, B., M. Biswal, S. Mohanty, and S. K. Nayak. 2019. In situ reactive compatibilization of polylactic acid (PLA) and thermoplastic starch (TPS) blends; synthesis and evaluation of extrusion blown films thereof. *Ind. Crops. Prod.* 141:111748. doi:10.1016/j.indcrop.2019.111748

[20] Müller, P., J. Bere, E. Fekete, J. Móczó, B. Nagy, M. Kállay, B. Gyarmati, and B. Pukánszky. 2016. Interactions, structure and properties in PLA/plasticized starch blends. *Polymer (Guildf).* 103:9–18. doi:10.1016/j.polymer.2016.09.031

[21] Martins, C., F. Vilarinho, A. Sanches Silva, M. Andrade, A. V. Machado, M. C. Castilho, A. Sá, A. Cunha, M. F. Vaz, and F. Ramos. 2018. Active polylactic acid film incorporated with green tea extract: Development, characterization and effectiveness. *Ind. Crops. Prod.* 123:100–110. doi:10.1016/j.indcrop.2018.06.056

[22] Ferri, J. M., O. Fenollar, A. Jorda-Vilaplana, D. García-Sanoguera, and R. Balart. 2016. Effect of miscibility on mechanical and thermal properties of poly (lactic acid)/polycaprolactone blends. *Polym. Int.* 65:453–463. doi:10.1002/pi.5079

[23] Kumar, B., M. Castro, and J. F. Feller. 2012. Poly (lactic acid)-multi-wall carbon nanotube conductive biopolymer nanocomposite vapour sensors. *Sensors Actuat, B Chem.* 161:621–628. doi:10.1016/j.snb.2011.10.077

[24] Nisa, N.,. B. Mohammad, A. Arsad, H. Jin, and N. Ngadi. 2021. Influences of pristine carbon nanotube on the rheological properties of compatibilized polylactic acid/natural rubber nanocomposite. *Mater. Today Proc.* 39:951–955. doi:10.1016/j.matpr.2020.04.211

[25] She, D., J. Dong, J. Zhang, L. Liu, Q. Sun, Z. Geng, and P. Peng. 2019. Development of black and biodegradable biochar/gutta percha composite films with high stretchability and barrier properties. *Compos. Sci. Technol.* 175:1–5. doi:10.1016/j.compscitech.2019.03.007

[26] Dong, X., L. He, Y. Liu, and Y. Piao. 2018. Preparation of highly conductive biochar nanoparticles for rapid and sensitive detection of 17β-estradiol in water. *Electrochim. Acta.* 292:55–62. doi:10.1016/j.electacta.2018.09.129

[27] Tan, X., Y. Liu, G. Zeng, X. Wang, X. Hu, Y. Gu, and Z. Yang. 2015. Application of biochar for the removal of pollutants from aqueous solutions. *Chemosphere.* 125:70–85. doi:10.1016/j.chemosphere.2014.12.058

[28] Huggins, T., H. Wang, J. Kearns, P. Jenkins, and Z. J. Ren. 2014. Biochar as a sustainable electrode material for electricity production in microbial fuel cells. *Bioresour. Technol.* 157:114–119. doi:10.1016/j.biortech.2014.01.058

[29] Titirici, M. M., R. J. White, C. Falco, and M. Sevilla. 2012. Black perspectives for a green future: Hydrothermal carbons for environment protection and energy storage. *Energy. Environ. Sci.* 5:6796–6822. doi:10.1039/c2ee21166a

[30] de Oliveira, P. R., C. Kalinke, J. L. Gogola, A. S. Mangrich, L. H. M. Junior, and M. F. Bergamini. 2017. The use of activated biochar for development of a sensitive electrochemical sensor for determination of methyl parathion. *J. Electroanal. Chem.* 799:602–608. doi:10.1016/j.jelechem.2017.06.020

[31] Dong, X., L. He, H. Hu, N. Liu, S. Gao, and Y. Piao. 2018. Removal of 17B-estradiol by using highly adsorptive magnetic biochar nanoparticles from aqueous solution. *Chem. Eng. J.* 352:371–379. doi:10.1016/j.cej.2018.07.025

[32] Qu, W., L. Wei, Z. Ma, and J. Julson. 2012. Fast pyrolysis of corn stover and sawdust in a novel reactor. *Am. Soc. Agric. Biol. Eng. Annu. Int. Meet. 2012, ASABE 2012* 3:2364–2378.

[33] Sobhan, A., J.-H. Oh, M.-K. Park, and J. Lee. 2018. Detection of peanut allergen ara h 6 in commercially processed foods using a single-walled carbon nanotube–based biosensor. *J. AOAC Int* 101:1558–1565. doi:10.5740/jaoacint.18-0041

[34] Sobhan, A., J. Lee, M. K. Park, and J. H. Oh. 2019. Rapid detection of Yersinia enterocolitica using a single–walled carbon nanotube-based biosensor for kimchi product. *LWT.* 108:48–54. doi:10.1016/j.lwt.2019.03.037

[35] Genovese, M., J. Jiang, K. Lian, and N. Holm. 2015. High capacitive performance of exfoliated biochar nanosheets from biomass waste corn cob. *J. Mater. Chem. A.* 3:2903–2913. doi:10.1039/C4TA06110A

[36] Smith, M. W., I. Dallmeyer, T. J. Johnson, C. S. Brauer, J. S. McEwen, J. F. Espinal, and M. Garcia-Perez. 2016. Structural analysis of char by raman spectroscopy: Improving band assignments through computational calculations from first principles. *Carbon N. Y.* 100:678–692. doi:10.1016/j.carbon.2016.01.031

[37] Chowdhury, Z. Z., M. Ziaul Karim, M. A. Ashraf, and K. Khalid. 2016. Influence of carbonization temperature on physicochemical properties of biochar derived from slow pyrolysis of durian wood (durio zibethinus) sawdust. *BioResources.* 11:3356–3372. doi:10.15376/biores.11.2.3356-3372

[38] Elnour, A. Y., A. A. Alghyamah, H. M. Shaikh, A. M. Poulose, S. M. Al-Zahrani, A. Anis, and M. I. Al-Wabel. 2019. Effect of pyrolysis temperature on biochar microstructural evolution, physicochemical characteristics, and its influence on biochar/polypropylene composites. *Appl. Sci* 9:7–9.

[39] Jia, Y., S. Shi, J. Liu, S. Su, Q. Liang, X. Zeng, and T. Li. 2018. Study of the effect of pyrolysis temperature on the Cd2+ adsorption characteristics of biochar. *Appl. Sci.* 8:1019.

[40] Chaichi, M., M. Hashemi, F. Badii, and A. Mohammadi. 2017. Preparation and characterization of a novel bionanocomposite edible film based on pectin and crystalline nanocellulose. *Carbohydr. Polym.* 157:167–175. doi:10.1016/j.carbpol.2016.09.062

[41] Yang, C., H. Tang, Y. Wang, Y. Liu, J. Wang, W. Shi, and L. Li. 2019. Development of PLA-PBSA based biodegradable active film and its application to salmon slices. *Food Packag. Shelf. Life.* 22:100393.

[42] Sobhan, A., K. Muthukumarappan, L. Wei, T. Van Den Top, and R. Zhou. 2020. Development of an activated carbon-based nanocomposite film with antibacterial property for smart food packaging. *Mater. Today. Commun.* 23:101124. doi:10.1016/j.mtcomm.2020.101124

[43] Sobhan, A., J.H. Oh, M.K. Park, S. W. Kim, C. Park, and J. Lee. 2018. Single walled carbon nanotube-based biosensor for detection of peanut allergy-inducing protein ara h1. *Korean J. Chem. Eng.* 35:172–177. doi:10.1007/s11814-017-0259-y

[44] Zhang, B., S. Ye, G. Xiao, and D. Dong. 2015. Identification of beef spoilage via the analysis of volatiles using long optical-path fourier transform infrared spectroscopy. *Anal. Methods.* 7:5891–5897. doi:10.1039/C5AY00033E

[45] Eom, K. H., K. H. Hyun, S. Lin, and J. W. Kim. 2014. The meat freshness monitoring system using the smart RFID tag. *Int. J. Distrib. Sens. Networks.* 10:591812. doi:10.1155/2014/591812

[46] Swe, M. M., T. Eamsa-Ard, T. Srikhirin, and T. Kerdcharoen. 2019. Monitoring the freshness level of beef using nanocomposite gas sensors in electronic nose. *2019 IEEE Int. Conf. Consum. Electron. - Asia. (ICCE-Asia)* 2019:100–103.

[47] Travlou, N. A., M. Seredych, E. Rodríguez-Castellón, and T. J. Bandosz. 2015. Activated carbon-based gas sensors: Effects of surface features on the sensing mechanism. *J. Mater. Chem. A.* 3:3821–3831. doi:10.1039/C4TA06161F